Parameterized Dynamic Range Reduction for UWB SAR Image

Chao Li and Yue-Li Li
College of Electronic Science and Engineering
National University of Defense Technology, Changsha, China

Abstract— The visualization of ultra wide bandwidth synthetic aperture radar (UWB SAR) image data involves mapping from high dynamic range amplitude values to gray values of a lower dynamic range display device. In order to compress dynamic range of the UWB SAR image data appropriately, we examine several different dynamic range reduction techniques and come up to a new method with better visualization performance. This new arithmetical technique is analyzed based on the 3σ measurement and the amended mapping function. Compared with the original method, the new method has higher computational efficiency with the dark pixels are stretched appropriately and the bright details are well preserved.

1. INTRODUCTION

Low-frequency ultra-wide bandwidth synthetic aperture radar (UWB SAR) is a new domain, which combines the ultra-wideband technology with synthetic aperture radar imaging technology. However, it is more difficult for researchers to obtain useful information from the UWB SAR images due to their high dynamic range and great quantity of calculation [1]. Therefore, developing a fast visual method for the UWB SAR amplitude values is essentially important and necessary.

In the UWB SAR images, corner reflectors, which are used for calibration and geocoding purposes, generate a large dynamic range of amplitude values. Therefore the dynamic range compression is a crucial step in the processing. There are logarithmic transformation [2], linear mapping and many other traditional methods that are used in dealing with the data of UWB SAR images. Generally, the dynamic range of primary amplitude values is typically much wider than conventional display devices. The logarithmic transformation may map a great number of amplitude values in one same gray level. All information in similar amplitude values is lost when using this method. In order to reserve more information in images, some researchers have proposed partial linear mapping method for UWB SAR images. This method divides the gray values into different parts by previous experience. However, when the input date changed the original divided model may not available. So, if we want to process the UWB SAR data real-time, we need to explore a new visual method.

In this paper, we proposed a fast visualization method based on the idea that the 3σ measurement can reduce the impact of intense echo signal and has a good performance in dynamic range reduction.

This paper is developed as follows. The Section 2 introduces commonly used methods for the SAR image data visualization. The Section 3 analyzes the distribution of UWB SAR image data and presents a fast visualization method for UWB SAR images visualization. The Section 4 compares the performance of the traditional visual methods with the new method by simulation and then reaches a conclusion that the proposed method is adaptive, improve the visibility of local details, and suit for real-time visualization system.

2. TRADITIONAL VISUALIZATION METHODS

2.1. Logarithmic Mapping

Logarithmic mapping is often used with SAR data. It can be defined as:

$$L_d(x, y) = \frac{\log(1 + cA(x, y))}{\log(1 + c)} \tag{1}$$

where the parameter c controls the overall brightness of the result and $A(x, y)$ is amplitude values. Generally, the amplitude range is often partially mapped to gray levels, and the values outside this range are clipped to black or white. It is obvious this method may map a large number of amplitude values in one same gray level while the primary dynamic range of image data is much larger than display devices. Therefore, all information in similar amplitude values is lost when using this method.

2.2. Partial Linear Mapping

Linear mapping from amplitude image data to gray levels is only usable when a relatively range of the amplitude values has been determined and values outside of this range are clipped to black or white. To make better use of the available gray level range, the method divides the gray values into different parts by previous experience before mapping. It is dropped as follow.

$$L_d(x,y)=\begin{cases} k_1A(x,y)+b_1 & 0\le A(x,y)\le f_1 \\ k_2A(x,y)+b_2 & f_1\le A(x,y)\le f_2 \\ k_3A(x,y)+b_3 & f_2\le A(x,y)\le f_3 \end{cases} \tag{2}$$

where k_1, k_2 and k_3 are parameters of different part of gray levels. The process of implementation is difficult because the original divided model may not available when the input date changed. Therefore we need to research a new real-time visualization method for UWB SAR data.

3. THE NEW VISUALIZATION METHOD FOR UWB SAR IMAGES

3.1. Statistical Property of UWB SAR Images

A notable feature of the low-frequency UWB SAR images is that the images have a large number of speckles due to the interaction of echo electromagnetic waves [3]. Goodman has proposed a statistical distribution model from researching the laser speckles [4]. With a similar theory, the statistical distribution model also demonstrates the statistical property of UWB SAR images. The reflectivity of each pixel in complicated UWB SAR image is defined as follows:

$$s=a+jb \tag{3}$$

Here, the real part and imaginary part both submit to zero-mean Gaussian distribution with equal variances and independent variables. The basic resolution unit of UWB SAR images can be viewed as a series of echo signals. According to the central limit theorem, the joint probability density function is defined as [5]:

$$p(a,b)=\frac{1}{2\pi\sigma^2}\exp\left[-\frac{\left(a^2+b^2\right)}{2\sigma^2}\right] \tag{4}$$

So the magnitude of the low-frequency UWB SAR image data submits to

$$p(x)=\left(\frac{x}{\sigma_0^2}\right)\exp\left(-\frac{x^2}{2\sigma_0^2}\right) \tag{5}$$

this is the Rayleigh distribution, where the σ_0^2 is the variance of the UWB SAR image data.

3.2. Power Transformation Principles

From the above discussion we are able to find out that the distribution of UWB SAR image data submits to the Rayleigh distribution. In order to change the distribution, a modified method based on power transformation is proposed. The 3σ measurement, as we all know, is widely used in screening engineering data. When using the basic principle, the date which later will be screened must submit to Gaussian distribution.

In this case, the power transformation is [6]

$$Y=X^v,\quad 0<v<1, \tag{6}$$

where X is the original data, Y is the transformed data, and v is the coefficient of transformation. Assuming A is a vector; we can get the standard secondary matrix:

$$d^2=(A-M)^{\mathrm{T}}\Sigma^{-1}(A-M)=Z^{\mathrm{T}}Z=\sum_{i=1}^{n}z_i^2 \tag{7}$$

where M and $\sum$ are the mean and covariance matrix, respectively. $Z=B^{\mathrm{T}}(A-M)^{\mathrm{T}}\Sigma^{-1}(A-M)$, $B=\Sigma^{-1/2}$, $E\{z_i\}=0$, $\mathrm{var}\{z_i\}=0$.

It is obvious that the d^2 submits to Chi-square distribution with n degrees of freedom.

$$\begin{aligned} E\left\{d^2\right\}&=n,\\ \mathrm{var}\left\{d^2\right\}&=2n. \end{aligned} \tag{8}$$

When $\{z_i\}$ is uncorrelated, the variance of d^2 is

$$\text{var}\left\{d^2\right\} = \gamma n \tag{9}$$

where $\gamma = E\{z_i^4\} - nE\{z_i^2\} = E\{z_i^4\} - n$.

Alternatively, we can calculate γ using this method [7]:

$$\gamma = \frac{E\left\{(y-\bar{y})^4\right\}}{E^2\left\{(y-\bar{y})^2\right\}} = \frac{E\left\{y^4\right\} + 6E\left\{y^2\right\}E^2\{y\} - 4E\left\{y^2\right\}E\{y\} - 3E^4\{y\}}{\left[E\left\{y^2\right\} - E^2\{y\}\right]^2} \tag{10}$$

where $E(y^n) = (\sqrt{2}\alpha)^{nv}\Gamma[nv/2+1]$.

As a result, we can get a value of 0.87 for v when $\gamma = 2$. Using this value, we are able to transform the distribution of the UWB SAR images data into Rayleigh distribution conveniently.

3.3. 3σ Measurement

The 3σ measurement is widely applied in screening engineering data. The basic principle is that the data must submit to Gaussian distribution when we use this method. In order to use the 3σ measurement in screening UWB SAR images data, we can utilize the power transformation, which has been discussed in the paper.

In the low-frequency UWB SAR images, the pixels with high intensity are in very limited amounts, yet the range of these pixels is extremely wide. The 3σ measurement regards some pixels with extremely high intensity as singular values. In this way, the high dynamic range of UWB SAR image data can be reduced adaptively.

Assume pixels in UWB SAR image' amplitude values are y_{ij} $(i \in [1, M], j \in [1, N])$. Therefore, the 3$\sigma$ measurement can be written as below:

$$|y_{ij} - \bar{y}| \geq 3s \tag{11}$$

where $\bar{y}$ is the mean and S is the variance. As a result, we can find the mapping boundary with this formula. A comparison between original amplitude values and new dates handled by 3σ measurement is shown in Fig. 1.

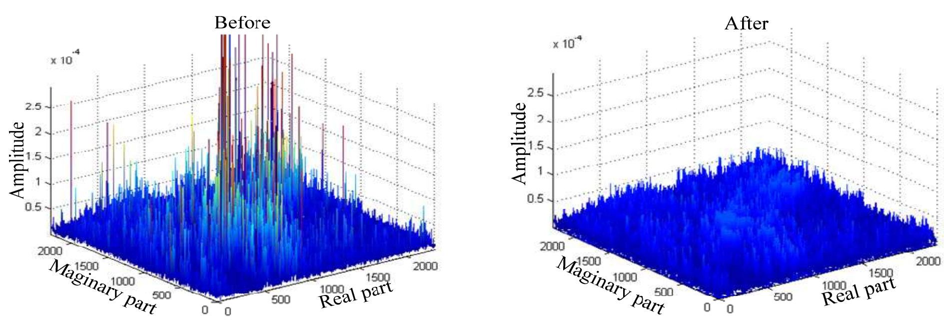

Figure 1: A comparison between different data.

Composed of low frequency UWB SAR image amplitude data, the Fig. 1 displays the range and tendency of the image amplitude. The influence of the strong echo signals is reduced while the small signals are well preserved using the 3σ measurement.

3.4. Amended Mapping Function

From the analysis discussed above, we know that the number of pixels with high intensity is limited when using the 3σ measurement. In a high contrastive visual image, the components of the histogram cover a wider range of the gray scale and extend further so that the PDF of the intensity levels is not too far from the log-normal distribution. Therefore, the lognormal distribution should be the target distribution of the transformed images. In this paper, we use the amended mapping function to achieve the transformation. It is defined as:

$$h = 255\frac{\exp(z) - 1}{\exp(z_m) - 1} \tag{12}$$

where, z is the UWB SAR images data after the 3σ measurement is applied, and z_m is the maximum of z. This mapping function is monotonically increasing; hence it is known that the brighter pixels in the displayed result are caused by the larger amplitude values.

In the UWB SAR images, the major features of interest are the peaks in the data that have considerably greater amplitude than the surrounding region. We utilize the following method to reduce the dynamic accordingly:

- Change the distribution of original UWB SAR image data using power transformation principles.
- Decrease the dynamic range of UWB SAR amplitude values by the 3σ measurement.
- Map the amplitude values to gray levels by using formula 12.

With the use of the dynamic range reduction processing, the gray level of peaks in UWB SAR image data are still emphasized peaks in UWB SAR amplitude values, although this method decreases the amplitude of these peaks.

3.5. Quality of UWB SAR Images

Equivalent Noise Level (ENL) [8] , as a variable to measure the relative intensity of SAR image speckle noise is defined as

$$ENL = \frac{E^2(R)}{\mathrm{var}(R)} \tag{13}$$

where $E(R)$ and $\mathrm{var}(R)$ are the mean and variance of UWB SAR gray images, respectively.

In the Human Visual System (HVS) [9], on one hand, the more central the position of pixel in UWB SAR images is, the more important it is. On the other hand, the HVS is also sensitive to contrast. Therefore, the indicator of HVS can be expressed as

$$Q = \frac{1}{N} \times \sum_{i=1}^{N} Q_f(i) Q_0(i) \tag{14}$$

where Q_f is the position of pixels, Q_0 is the contrast, and N is the number of block pictures.

4. RESULT

To demonstrate the effectiveness of the proposed method, we would use the echo data obtained from the airborne UWB SAR system.

Figure 2(a) shows the visualization result from the logarithmic transformation. Fig. 2(b) is the gray value histogram. Apparently, the result is not making the best use of gray scales.

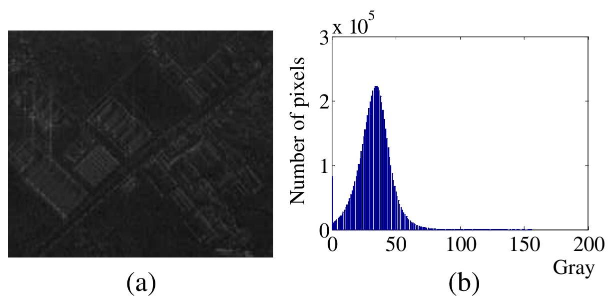

(a) (b)

Figure 2: The UWB SAR data visualization result using logarithmic transform.

With the linear mapping method, the visualization result of UWB SAR amplitude values is shown in Fig. 3(a), which is different from Fig. 2(a). It is obvious that most of pixels in the image share the same gray values from the histogram in the Fig. 3(b). Therefore, some details of the image with similar amplitude values are disappeared.

The visualization result of UWB SAR data is based on the proposed method in this paper shown in Fig. 4(a), with the histogram being shown in Fig. 4(a). From the Fig. 4, we could see that the histogram covers a wider range of gray scale and details in the emphasized image. Therefore, it is relatively convenient for researchers to obtain useful information.

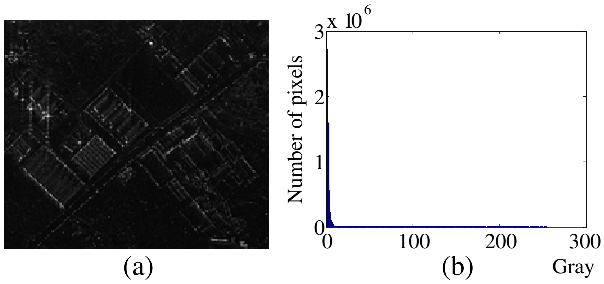

Figure 3: The UWB SAR data visualization result using linear mapping.

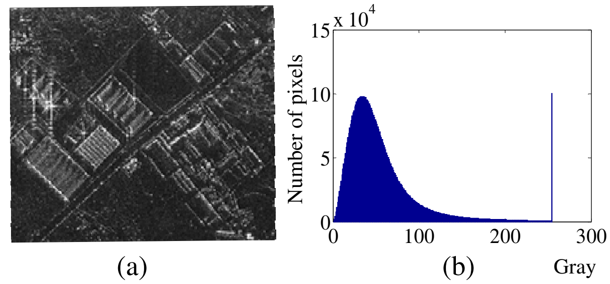

Figure 4: The UWB SAR data visualization result using proposed method.

Table 1: Quality of UWB SAR images.

		Mountains	**Urban**	**Roads**	**Mean**
logarithmic transform	time	10.1 s	12.2 s	11.5 s	11.267 s
	ENL	1.60	1.65	1.70	1.65
	HVS	0.5556	0.6445	0.4523	0.5508
linear mapping	time	8.3 s	8.9 s	9.5 s	8.3 s
	ENL	0.34	0.66	0.54	0.51
	HVS	0.6678	0.7022	0.6955	0.6885
proposed method	time	7.5 s	7.9 s	7.1 s	7.5 s
	ENL	1.97	2.33	2.13	2.14
	HVS	0.8889	0.9012	0.9123	0.9008

In order to measure the processing speed and image quality of the fast visualization algorithm proposed in this paper, mountains, urban, and roads are selected in the experiment. The result is shown in Table 1.

From the discussion above, it is obvious that the fast visualization algorithm is not only better than the ordinary methods, but also more suitable for real-time processing.

5. CONCLUSIONS

This paper presents a new fast visualization method for UWB SAR images based on 3σ measurement. Compared with the original method, this new method takes less time. In addition, the dark pixels are stretched appropriately, and the bright details are well preserved. The performance of the algorithm has been illustrated by the airborne UWB SAR data.

REFERENCES

1. An, D. X., Y. H. Li, X. T. Huang, X. Y. Li, and Z. M. Zhou, "Performance evaluation of frequency-domain algorithms for chirped low frequency UWB SAR data processing," *IEEE Journal of Selected Topics in Applied Earth Observations and Remote Sensing*, Vol. 7, No. 2, 678–690, Feb. 2014.
2. Lamber, M., H. Nies, and A. Kolb, "Interactive dynamic range reduction for SAR images," *Geoscience and Remote Sensing Letters*, Vol. 5, No. 3, 507, 2008.
3. Oliver, C. and S. Quegan, *Understanding Synthetic Aperture Radar Images*, [S.l.]: Sci Tech Publishing, 2004.
4. Goodman, J., *Statistical Properties of Laser Speckle Patterns Laser Speckle and Related Phenomena*, 9–75, Springer-Verlag, Berlin, 1975.
5. Zhou, G., W. An, J. Yang, and H. Zhong, "A visualization method for SAR images," *IGARSS*, 374, 2011.
6. Kukunage, K., *Introduction to Statistical Pattern Recognition*, 1990.
7. Jiao, L., X. Zhang, B. Hou, H. Wang, and F. Liu, *Intelligent SAR Image Processing and Interpretation*, Science Press, Beijing, 2008.
8. Wang, Z., L. G. Lu, and A. C. Bovik, "Foveation scalable video coding with automatic fixation selection," *IEEE Transactions on Image Processing*, Vol. 12, No. 2, 243–254, 2003.
9. Mannos, J. L. and D. J. Sakrison, "The effects of a visual fidelity criterion on the encoding of images," *IEEE Transactions on Information Theory*, Vol. 20, No. 4, 525, 1974.